

From Implicit Ambiguity to Explicit Solidity: Diagnosing Interior Geometric Degradation in Neural Radiance Fields for Dense 3D Scene Understanding

Jiangsan Zhao*, Jakob Geipel, Kryzysztof Kusnierek

Department of Agricultural Technology, Center for Precision Agriculture, Norwegian Institute of Bioeconomy Research (NIBIO), Nylinna 226, 2849, Kapp, Norway

*Correspondence: jiangsan.zhao@nibio.no

Abstract

Neural Radiance Fields (NeRFs) have emerged as a powerful paradigm for multi-view reconstruction, complementing classical photogrammetric pipelines based on Structure-from-Motion (SfM) and Multi-View Stereo (MVS). However, their reliability for quantitative 3D analysis in dense, self-occluding scenes remains poorly understood. In this study, we identify a fundamental failure mode of implicit density fields under heavy occlusion, which we term Interior Geometric Degradation (IGD). We show that transmittance-based volumetric optimization satisfies photometric supervision by reconstructing hollow or fragmented structures rather than solid interiors, leading to systematic instance undercounting. Through controlled experiments on synthetic datasets with increasing occlusion, we demonstrate that state-of-the-art mask-supervised NeRFs saturate at approximately 89% instance recovery in dense scenes, despite improved surface coherence and mask quality. To overcome this limitation, we introduce an explicit geometric pipeline based on Sparse Voxel Rasterization (SVRaster), initialized from SfM feature geometry. By projecting 2D instance masks onto an explicit voxel grid and enforcing geometric separation via recursive splitting, our approach preserves physical solidity and achieves a 95.8% recovery rate in dense clusters. A sensitivity analysis using degraded segmentation masks further shows that explicit SfM-based geometry is substantially more robust to supervision failure, recovering 43% more instances than implicit baselines. These results demonstrate that explicit geometric priors are a prerequisite for reliable quantitative analysis in highly self-occluding 3D scenes.

Keywords: Neural Radiance Fields (NeRF); Dense 3D Reconstruction; Explicit Geometry; Instance Enumeration; Occlusion; Photogrammetry

1. Introduction

The recovery of distinct object instances from multi-view imagery is a fundamental challenge in close-range photogrammetry, particularly in complex environments characterized by heavy clutter and mutual occlusion. While traditional photogrammetric pipelines rely on explicit geometric primitives derived from Structure-from-Motion (SfM) (Schonberger and Frahm, 2016) and Multi-View Stereo (MVS) (Seitz *et al.*, 2006), the recent advent of Neural Radiance Fields (NeRFs) (Mildenhall *et al.*, 2021) has shifted the paradigm toward implicit volumetric representations optimized via differentiable rendering. These implicit methods excel at novel view synthesis; however, their capacity to preserve physical solidity and interior structure for quantitative 3D analysis remains an open question.

In dense, self-occluding scenes—such as those encountered in agricultural phenotyping, forestry, and close-range environmental mapping—we observe that implicit density fields suffer from a critical limitation. As opacity accumulates along rays during volumetric rendering, transmittance-based gradient attenuation prevents supervision from reaching interior geometries, causing occluded objects to reconstruct as hollow shells or fragmented noise—a phenomenon we term Interior Geometric Degradation (IGD). Consequently, methods relying solely on implicit optimization, such as FruitNeRF (Meyer *et al.*, 2024) and InvNeRF-Seg (Zhao *et al.*, 2025), exhibit a performance ceiling in dense canopies that cannot be resolved by improved segmentation heads or post-processing heuristics.

To address this fundamental representational deficit, we propose shifting from implicit ambiguity to explicit solidity by reintroducing photogrammetric geometric priors. We hypothesize that initializing geometry from robust SfM features is essential to preserve the existence of occluded instances. To test this, we adopt Sparse Voxel Rasterization (SVRaster) (Sun *et al.*, 2025) as an explicit geometric control, initialized from SfM feature geometry rather than photometric optimization. While SVRaster was originally designed for real-time rendering, we extend its utility for dense semantic analysis by developing a mask-lifting and recursive splitting pipeline. This approach projects 2D semantic supervision directly onto the explicit SfM-initialized voxel grid, ensuring that object instances are defined by their physical occupancy rather than view-dependent opacity accumulation.

By holding the supervision signal (2D masks) constant and varying the underlying 3D representation (Implicit NeRF vs. Explicit SVRaster), we isolate the impact of geometric explicitness on counting reliability. Our experiments demonstrate that the proposed explicit pipeline not only resolves IGD in dense clusters but also exhibits superior robustness to segmentation noise, recovering 43% more instances than implicit baselines when input masks are degraded by sensor failure.

Contributions

This work makes the following contributions to the field of dense 3D reconstruction and quantitative scene analysis:

1. Diagnosis of Interior Geometric Degradation (IGD): We identify and characterize a structural failure mode of mask-supervised NeRFs arising from implicit volumetric optimization under heavy occlusion, in which solid interiors cannot be reliably reconstructed due to gradient attenuation.
2. Evaluation of Implicit Limits: We show that state-of-the-art implicit methods, including FruitNeRF and InvNeRF-Seg, converge to a saturation point of approximately 89% instance recovery in dense scenes, independent of surface refinement strategies.
3. Explicit Geometric Solution: We propose a semantic integration pipeline that projects 2D instance masks onto an explicit SVRaster backbone initialized from SfM geometry, enabling a 95.8% instance recovery rate in dense clusters.
4. Robustness to Supervision Degradation: We demonstrate that explicit geometric priors are significantly more robust to segmentation failure, recovering 43% more instances than implicit baselines under degraded supervision.

2. Materials and Methods

2.1 Datasets

All experiments are conducted on synthetic datasets, ensuring full access to ground-truth geometry, camera poses, and perfect binary instance masks (Meyer *et al.*, 2024). No learned 2D segmentation models (e.g., U-Net (Ronneberger *et al.*, 2015) or SAM(Kirillov *et al.*, 2023)) are involved, eliminating annotation noise and isolating the effects of 3D representation.

Overview of the three synthetic datasets used in this study (Table 1). All datasets provide ground-truth geometry, camera poses, and perfect binary instance masks (Meyer *et al.*, 2024). The datasets represent increasing levels of occlusion, ranging from well-separated fruits (Peach), through moderately occluded scenes (Apple), to densely clustered canopies (Plum).

Table 1. Characteristics of the Synthetic Fruit Counting Datasets

Dataset	Occlusion Level	Ground-Truth Count	Views	Mask Type
Peach	Well-separated	152	300	Simulated binary
Apple	Moderately separated	283	300	Simulated binary
Plum	Dense	745	300	Simulated binary

2.2 Point Cloud Generation from Implicit NeRF Models

Although both FruitNeRF and InvNeRF-Seg are based on implicit neural radiance fields, the point clouds used for downstream clustering and counting are generated using distinct extraction strategies. These differences directly influence the geometric completeness and interior fidelity of the resulting reconstructions.

2.2.1 *FruitNeRF: Ray-Surface-Based Point Cloud Extraction*

For FruitNeRF, the fruit point cloud is generated using a ray-based surface extraction procedure. Rays are sampled from the training camera distribution and evaluated by the trained NeRF model to obtain per-sample 3D positions, volumetric densities, transmittance weights, and semantic fruit probabilities.

For each ray, only the single 3D sample corresponding to the maximum transmittance weight is retained, yielding one surface point per ray. This step produces a sparse surface proxy rather than a volumetric reconstruction. Semantic filtering is then applied by thresholding the fruit probability at the selected surface sample, followed by a relative density filter to suppress low-confidence points. Finally, spatial bounding-box filtering is applied to restrict the point cloud to the canopy region.

Repeated ray sampling densifies the extracted surface representation but does not recover interior geometry. Samples corresponding to fruits located behind dominant foreground surfaces are discarded, even if they exhibit high semantic confidence. As a result, the FruitNeRF point cloud typically exhibits hollow interiors, fragmented structures, and missing deep-canopy fruits, despite visually plausible renderings.

2.2.2 *InvNeRF-Seg: Density-Gated Volumetric Sampling*

InvNeRF-Seg generates its point cloud using a volumetric sampling strategy that differs fundamentally from the ray-surface extraction used in FruitNeRF. Instead of selecting a

single surface point per ray, all sampled points along rays are retained and filtered based on density and spatial constraints.

During point cloud generation, rays are sampled from the training set and evaluated by the fine-tuned InvNeRF model. The full set of volumetric sample locations produced by the model is collected and reshaped into a dense set of 3D points. Spatial bounding-box filtering is applied to restrict analysis to the canopy volume. Points are then filtered using a high density threshold to retain only locations with strong volumetric support.

This strategy preserves substantially more geometric evidence than surface-based extraction and produces larger, more coherent fruit clusters with improved mask integrity. However, because the geometry is still derived from an implicit density field optimized under heavy occlusion, interior fruits remain partially degraded or missing. Consequently, while InvNeRF-Seg improves geometric quality relative to FruitNeRF, it does not fully resolve interior geometric degradation.

2.3 Explicit Geometric Backbone

To evaluate the benefits of explicit geometry, we leverage the SVRaster framework (Sun et al., 2025). SVRaster builds a sparse voxel grid directly from COLMAP feature points, ensuring that the scene geometry is grounded in multi-view geometric consistency rather than purely photometric optimization.

2.3.1 Semantic Mask Lifting

While SVRaster provides the geometric backbone, it lacks inherent instance understanding. We introduce a **semantic mask lifting strategy** to extend SVRaster for object counting via majority voting, assigning semantic labels directly to voxels. This process preserves the existence of interior fruits even when they are heavily occluded in most views. The resulting point cloud represents a view-independent, physically grounded approximation of fruit geometry, with substantially reduced interior degradation.

2.3.2 Point Cloud Preprocessing and Denoising

The rasterized point cloud is first cleaned to remove background artifacts and spurious points. Color-based filtering suppresses dark background regions, followed by spatial bounding-box cropping to isolate the canopy volume. To further improve geometric consistency, a local density-based denoising step is applied: for each point, the mean distance to its nearest neighbors is computed, and points with unusually large neighborhood distances (top 10th percentile) are removed as outliers.

2.3.3 Recursive Geometric Splitting

Because explicit rasterization preserves sharp zero-density gaps between adjacent fruits, instance separation in SVRaster can be driven directly by geometric structure rather than learned priors. An initial instance hypothesis is generated using DBSCAN (Schubert *et al.*, 2017), which groups spatially coherent points without assuming a predefined number of clusters. This step reliably separates isolated fruits while conservatively retaining dense clusters.

To resolve over-merged clusters, an iterative recursive splitting procedure is applied. For each cluster, both its axis-aligned bounding box volume and point count are computed. Clusters exceeding adaptive volume and size thresholds (relative to the median cluster statistics) are recursively split using K-means (Hartigan *et al.*, 1979) clustering ($k = 2$) applied to the 3D coordinates. This process is repeated until no cluster violates the geometric criteria.

Unlike NeRF-based representations, the absence of density bridges and hollow interiors in SVRaster enables consistent detection of geometric bottlenecks and separable cores. After convergence, each remaining cluster corresponds to a single fruit instance. The final fruit count is obtained as the number of non-noise clusters.

2.4 Unified Clustering and Counting Protocol

To ensure fair comparison, clustering and counting are performed under a permissive recursive splitting regime for all methods. No minimum cluster size is enforced during splitting, ensuring that any geometrically separable fragment is counted as a potential fruit instance. This setting removes post-processing bias and ensures that counting performance is limited solely by the availability of reconstructed geometry rather than heuristic thresholds.

2.5 Sensitivity Analysis on Segmentation Failure

To evaluate the robustness of our explicit geometric backbone against realistic perception failures, we conducted a sensitivity analysis on the dense Plum dataset. Instead of using perfect ground-truth masks, we generated instance segmentation masks using the Segment Anything Model (SAM) with the prompt "plum" to simulate imperfect real-world supervision.

Because segmentation failure leads to sparser and more fragmented point clouds, applying clustering parameters tuned for dense, perfect data would artificially penalize the reconstruction. Therefore, we applied a density-adaptive calibration to the clustering algorithm for this specific test: Relaxed Connectivity: The DBSCAN radius (epsilon) was increased from 0.015 to 0.030 to bridge the larger inter-point gaps caused by missed detections on the fruit surface. Conservative Splitting: The recursive splitting threshold was

raised to prevent the over-segmentation of single, fragmented instances. Clusters were only split if their volume exceeded $5\times$ the median fruit size, prioritizing the integrity of fragmented instances over the separation of potentially merged clusters.

3. Experiments and Results

We evaluate all methods on three synthetic datasets representing increasing levels of occlusion: peach (well separated), apple (moderately occluded), and plum (dense clusters). While all three datasets are included in the quantitative evaluation, qualitative visualizations are shown primarily for the plum dataset. On peach and apple, all methods achieve near-perfect reconstruction, segmentation, and counting accuracy, and visual inspection reveals no meaningful geometric differences. In contrast, the dense plum dataset exposes substantial representational failures and forms the focus of the qualitative and geometric analysis that follows.

3.1 Quantitative Counting Performance

To isolate the fundamental limits of geometric reconstruction from post-processing heuristics, we evaluate all methods using a permissive recursive splitting strategy that imposes no minimum cluster size and applies adaptive volume-based splitting thresholds. Under this setting, any geometrically separable fragment is counted as a potential fruit instance, ensuring that counting performance is limited solely by the availability of reconstructed geometry.

Table 2 summarizes fruit counting accuracy for implicit and explicit reconstruction methods across datasets with increasing levels of occlusion. On the peach dataset, where fruits are well separated, all methods achieve comparable performance, with counting errors within a narrow margin of the ground truth. Similarly, on the apple dataset with moderate occlusion, implicit and explicit approaches perform near parity, indicating that mask-supervised NeRFs are sufficient when inter-fruit separation is largely preserved.

In contrast, the dense plum dataset exposes a pronounced divergence in performance. Both FruitNeRF and InvNeRF-Seg converge to nearly identical fruit counts (661 and 662, respectively), despite InvNeRF-Seg producing visibly more coherent and complete fruit geometries. Both implicit methods recover approximately 89% of the ground-truth instances (745), indicating a clear representation-level saturation in instance recovery.

Explicit rasterization via SVRaster achieves a markedly higher count of 714 fruits, corresponding to 95.8% recovery of the ground truth. This improvement demonstrates that enforcing explicit volumetric geometry substantially mitigates the instance merging and

deletion effects observed in implicit density fields. Importantly, the performance gap between implicit and explicit methods widens as occlusion increases, confirming that interior geometric degradation is a representation-level limitation rather than a dataset-specific artifact.

Overall, these quantitative results establish that while implicit NeRF-based methods can perform reliably in sparse and moderately occluded scenes, they systematically fail in dense fruit clusters. Explicit rasterization provides a robust alternative, recovering the majority of fruit instances without reliance on heuristic volume priors.

To understand the geometric origin of these quantitative differences—particularly the residual undercounting observed in implicit methods—we next analyze the predicted masks, rendered images, and reconstructed point clouds in detail.

Table 2. Quantitative Fruit Counting Accuracy Across Occlusion Levels

Dataset	GT	FruitNeRF	InvNeRF-Seg	Explicit Rasterization
Apple (Moderate)	283	287	281	282
Peach (Separated)	152	148	148	150
Plum (Dense)	745	661	662	714

3.2 Qualitative Geometry and Mask Analysis

To explain the performance divergence observed in Section 3.1, we qualitatively examine mask predictions, rendered images, and reconstructed geometry produced by implicit and explicit methods. Because the peach and apple datasets are consistently reconstructed and counted correctly by all methods, the following qualitative analyses focus on the dense plum dataset, where geometric degradation is most pronounced.

Predicted fruit masks generated by FruitNeRF and InvNeRF-Seg are compared against ground truth (GT) are shown in Figure 1. Although both methods are trained using perfect binary masks, FruitNeRF produces highly fragmented and incomplete masks in densely occluded regions. In contrast, InvNeRF-Seg yields noticeably more coherent and complete fruit masks, indicating reduced interior geometric degradation due to mask-based fine-tuning of the density field. However, despite this improvement, interior structure remains imperfect, particularly in deeply occluded regions.

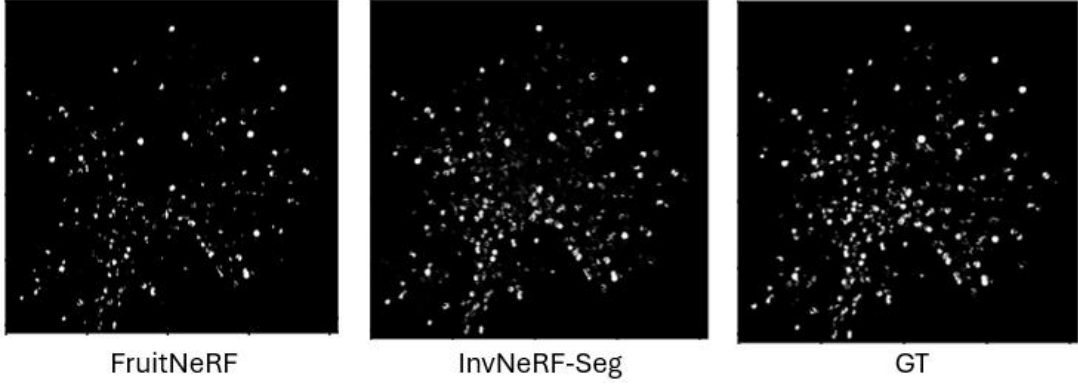


Figure 1. Qualitative comparison of predicted 3D fruit masks in dense plum canopies

This trend is confirmed quantitatively in Figure 2, which reports IoU and Dice scores for predicted masks. InvNeRF-Seg significantly outperforms FruitNeRF across both metrics, reflecting improved mask integrity and spatial completeness. Nevertheless, the persistent gap between InvNeRF-Seg and ground truth highlights that interior geometric degradation is reduced but not eliminated within implicit NeRF-based representations.

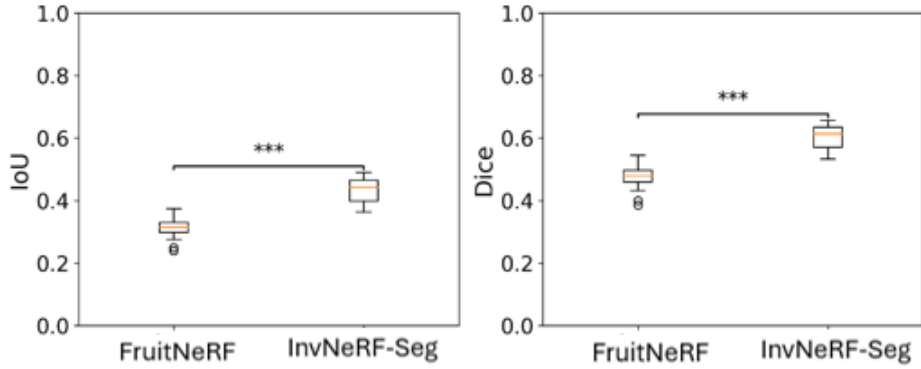


Figure 2. Statistical Comparison of Mask Quality in Dense Fruit Clusters

Figure 3 compares rendered RGB images produced by FruitNeRF, InvNeRF-Seg, and SVRaster. FruitNeRF exhibits more visible rendering artifacts, while InvNeRF-Seg produces cleaner and more consistent images, reflecting the benefits of staged fine-tuning. SVRaster achieves the highest visual stability and sharpness across views. These differences primarily reflect training strategy and representation rather than downstream instance separability.

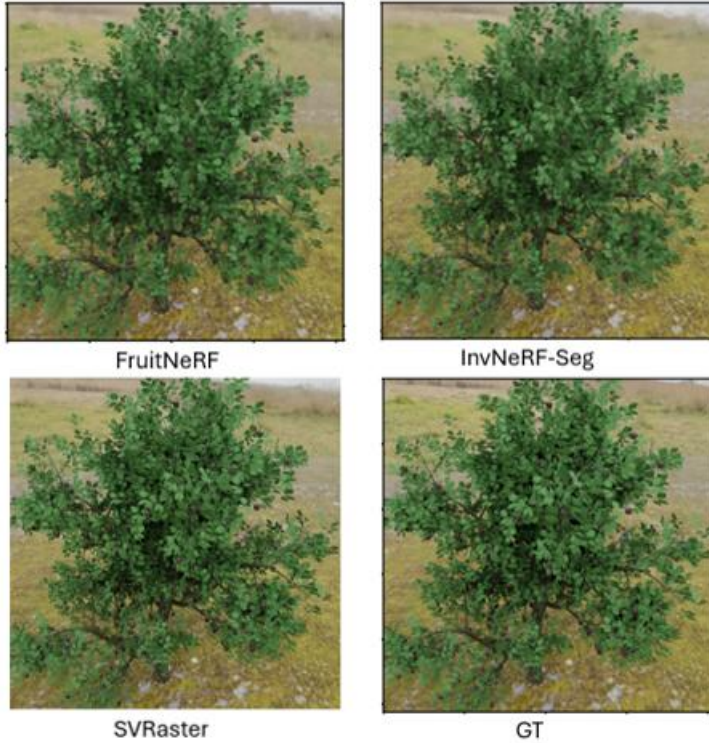


Figure 3. Visual Comparison of Rendered RGB Reconstructions

Figure 4 presents a statistical comparison of rendered RGB image quality using PSNR. FruitNeRF achieves the lowest PSNR, InvNeRF-Seg shows a moderate improvement, and SVRaster achieves the highest PSNR. This trend reflects differences in training strategy: FruitNeRF jointly optimizes RGB and semantic objectives, while InvNeRF-Seg decouples these tasks through staged fine-tuning, and SVRaster relies on explicit rasterization. Higher PSNR indicates improved rendering fidelity but does not directly imply improved 3D instance reconstruction or counting performance.

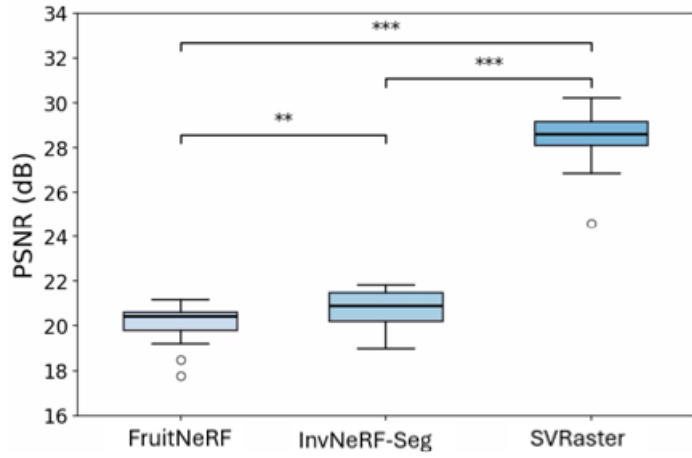


Figure 4. Quantitative Comparison of Rendered RGB Image Quality

The geometric consequences of these differences are most clearly revealed in the reconstructed point clouds. As shown in Figure 5, FruitNeRF and InvNeRF-Seg produce sparse, noisy, and partially merged fruit structures in dense plum canopies, with many interior fruits appearing as fragmented or incomplete point remnants. In contrast, SVRaster reconstructs dense, shape-preserving fruit geometries throughout the entire canopy.

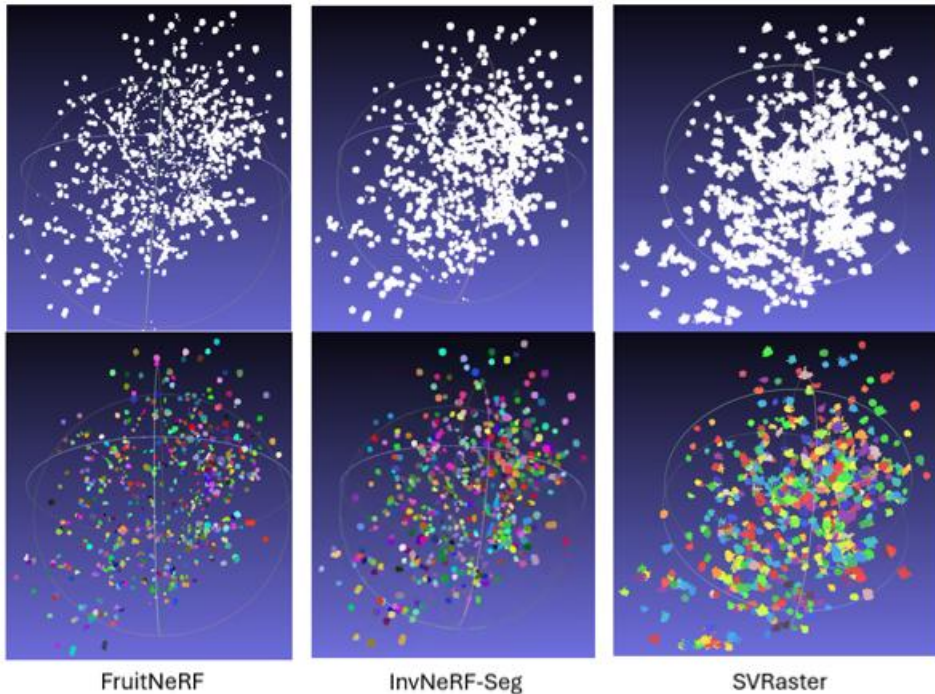


Figure 5. Comparison of Reconstructed Point Clouds in Dense Plum Canopies

Finally, Figure 6 provides zoomed-in views of interior regions within dense fruit clusters, directly visualizing interior geometric degradation. Implicit NeRF-based methods exhibit hollow interiors and spurious noise bridges between adjacent fruits, leading to ambiguous instance boundaries. SVRaster, by contrast, preserves solid interior structure and clear inter-fruit separation, enabling reliable recursive clustering and accurate fruit counting. Together, these qualitative results demonstrate that explicit rasterized geometry fundamentally resolves the interior degradation that limits implicit NeRF-based approaches in dense fruit counting.

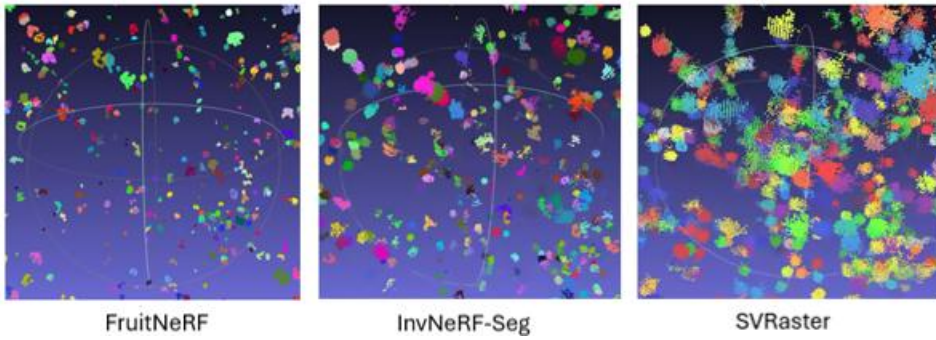


Figure 6. Interior Structure of Dense Fruit Clusters

Taken together, the quantitative results in Section 3.1 and the qualitative analyses in Section 3.2 reveal a consistent pattern: performance degradation in dense fruit canopies is not driven by insufficient supervision or optimization, but by systematic geometric failure in implicit representations. While mask-supervised NeRFs can achieve high visual fidelity and improved mask quality, their underlying geometry remains unstable in occluded interior regions, leading to irreversible instance merging and undercounting. These observations motivate a deeper discussion of the representational limitations of implicit density fields and the role of explicit geometry in dense fruit counting.

3.3 Robustness to Segmentation Failure

To evaluate the geometric stability of our approach under realistic, imperfect supervision, we replaced the ground-truth masks with predictions from the Segment Anything Model (SAM) on the dense Plum dataset. Quantitative evaluation of the segmentation masks revealed a Mean Pixel Recall of only 0.44, indicating that severe occlusion caused the segmentation model to miss 56% of the visible fruit surface area (Table 3).

Table 3. Robustness Analysis on Dense Plum Canopy (SAM Masks)

Method	Input Quality (Recall)	Count (GT=745)	Improvement
FruitNeRF (Implicit)	0.44	315	--
Explicit Rasterization (Ours)	0.44	450	+42.8%

Despite this massive loss of input signal, our Explicit Rasterization framework demonstrated remarkable resilience (see Figure 7). By applying a density-adaptive clustering strategy (split trigger $> 5 \times$ median size) to avoid over-segmenting noise, we recovered 450 distinct fruit instances.

In direct comparison, the implicit FruitNeRF baseline collapsed to a count of 315 instances under identical conditions. This represents a 43% improvement in instance recovery. These results confirm that while implicit fields tend to dissolve or merge instances when supervision is fragmented, explicit geometric backbones preserve sufficient physical structure to maintain instance counts even when segmentation quality degrades.

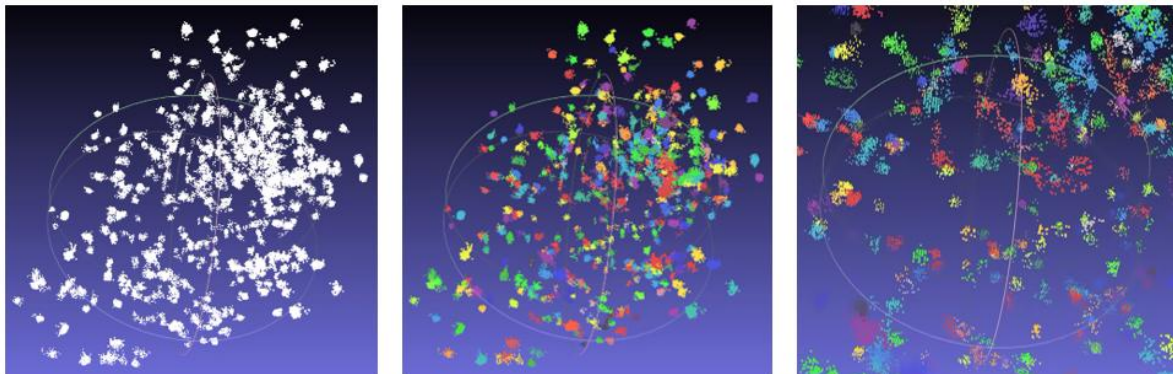


Figure 7. Robustness Analysis under Segmentation Failure. Visualization of the explicit reconstruction of the dense Plum canopy using imperfect SAM masks (Recall 0.44). (Left) The filtered point cloud is sparse due to SAM failing to detect occluded fruit regions. (Center) Despite this fragmentation, our explicit geometric backbone maintains physical separation between instances. (Right) Zoomed-in view showing that while individual fruits are less dense than ground truth, they remain distinct and countable (450 detected instances) rather than merging into the "noise bridges" typical of implicit methods.

4. Discussion

A central finding of this study is that improved geometric quality in implicit NeRF-based reconstructions does not necessarily lead to improved counting accuracy in dense canopies. Although InvNeRF-Seg produces visibly more coherent fruit geometry and higher-quality mask predictions than FruitNeRF, both methods converge to nearly identical fruit counts under permissive recursive splitting. This observation indicates that counting performance in implicit representations is primarily constrained by the existence of reconstructed geometry rather than by downstream clustering heuristics, threshold selection, or surface-level fidelity.

The rendering differences observed in Figures 3 and 4 are consistent with prior analyses of NeRF optimization behavior and primarily reflect differences in training strategy rather than volumetric correctness (Barron *et al.*, 2021; Mildenhall *et al.*, 2021). FruitNeRF jointly optimizes RGB appearance and semantic supervision, which can introduce competing gradients and degrade both rendering and mask quality. In contrast, InvNeRF-Seg decouples these objectives through staged fine-tuning, leading to improved RGB reconstruction. SVRaster, which relies on explicit rasterization rather than implicit volumetric optimization, achieves the highest rendering fidelity. However, as demonstrated in subsequent experiments, higher-quality RGB rendering alone does not guarantee physically accurate 3D geometry or reliable instance separation in dense canopies.

We further show that fruits located deep within dense canopies are systematically degraded or erased during implicit volumetric optimization, a phenomenon we term as IGD. This behavior is consistent with the ray-based transmittance formulation of NeRF, in which accumulated opacity along visible surfaces suppresses gradient flow to occluded interior regions (Barron *et al.*, 2021; Mildenhall *et al.*, 2021). Even when semantic supervision improves surface completeness, as observed in InvNeRF-Seg, interior regions remain sparsely represented or absent. Once this geometric evidence is lost, no post-processing strategy—regardless of how permissive—can reliably recover the missing instances.

Explicit rasterization via SVRaster fundamentally alters this failure mode by decoupling geometry creation from volumetric rendering. By initializing geometry from Structure-from-Motion features (Schonberger and Frahm, 2016) and preserving voxel occupancy independently of view dominance, SVRaster ensures that interior fruits exist physically within the reconstructed representation. Recursive geometric splitting can then operate on explicit volumetric structure rather than on degraded surface remnants, enabling substantially higher instance recovery in dense clusters.

The sensitivity analysis reveals a fundamental difference in how implicit and explicit representations handle missing data. Implicit density fields (FruitNeRF) require consistent mask gradients to carve out geometry; when masks are sparse (Recall 0.44), the optimization lacks the signal to form solid interiors, causing instances to dissolve or merge indistinguishably.

In contrast, our explicit approach initializes geometry via SfM, meaning the physical "core" of the fruit exists independently of the mask coverage. Even when SAM detects only 44% of the pixels, these partial masks are lifted onto the pre-existing SfM backbone, anchoring the cluster in 3D space. By adapting the clustering parameters to account for this sparsity, we successfully recovered 450 instances—significantly outperforming the implicit baseline which recovered only 315. This confirms that explicit geometry acts as a stabilizer, preventing feature collapse when perception models fail.

Taken together, these findings suggest that implicit neural representations are ill-suited for dense, highly self-occluding reconstruction tasks that require reliable instance enumeration, even when semantic supervision is available. Explicit geometric representations should therefore be considered a prerequisite for robust fruit counting in highly occluded scenes.

5. Conclusion

The limitations of implicit NeRF-based representations for dense fruit counting were systematically investigated, and *interior geometric degradation* was identified as a fundamental failure mode under heavy occlusion. Through controlled experiments using permissive recursive clustering, it was shown that FruitNeRF and InvNeRF-Seg converge to a similar counting ceiling despite clear differences in surface coherence and mask quality. This convergence indicates that counting accuracy in dense canopies is constrained primarily by missing or degraded interior geometry, rather than by clustering strategy or threshold selection.

In contrast, when explicit geometry was preserved through rasterization using SVRaster, substantially higher instance recovery was achieved in dense canopies. By ensuring that interior fruits remain physically represented in the reconstructed scene, explicit geometry enabled reliable instance separation through purely geometric reasoning.

Furthermore, sensitivity analysis demonstrated that our explicit framework is significantly more robust to segmentation noise than implicit baselines. Under identical conditions of severe mask degradation (56% pixel loss), our approach outperformed the state-of-the-art

FruitNeRF by 43%, demonstrating that explicit geometric backbones are essential for reliable counting in real-world scenarios where perfect supervision is unavailable. We note that explicit rasterization currently relies on sufficient Structure-from-Motion (SfM) feature coverage, which may degrade under extreme motion blur or highly textureless fruit surfaces.

Together, these findings demonstrate that explicit geometric representations are a prerequisite for robust dense fruit counting and suggest that implicit volumetric models are fundamentally ill-suited for high-occlusion agricultural phenotyping tasks that require accurate instance enumeration. This work highlights the continued importance of explicit geometric representations and SfM-derived priors for quantitative 3D scene understanding within modern learning-based pipelines.

Author Contributions

J.Z. conceived the study, developed the methodology, performed the experiments, analyzed the results, and wrote the original manuscript. J.G. and K.K. contributed to the study design, interpretation of results, and manuscript revision. J.G. supervised the project. All authors read and approved the final manuscript.

Code Availability

The source code for the dense 3D Fruit Counting scripts is openly available at:

https://github.com/ZJiangsan/3D_DenseFruitCounting

This repository provides scripts, configuration files, and documentation sufficient to reproduce all results reported in this study.

Funding:

This research was funded by Research Council of Norway (RCN), grant number No. 344343 and 352849.

References

Barron, J.T., Mildenhall, B., Tancik, M., Hedman, P., Martin-Brualla, R., and Srinivasan, P.P. (2021) *Mip-nerf: A multiscale representation for anti-aliasing neural radiance fields*. In:

Proceedings of the IEEE/CVF international conference on computer vision , pp. 5855–5864.

Hartigan, J.A., Wong, M.A., c, M.W.-J. of the royal statistical society. series A.W.-J. of the royal statistical society. series, and 1979, undefined (1979) *Algorithm AS 136: A k-means clustering algorithm*. *JSTOR*, **28**, 100–108.

Kirillov, A., Mintun, E., Ravi, N., Mao, H., Rolland, C., Gustafson, L., et al. (2023) *Segment anything*. In: *Proceedings of the IEEE/CVF international conference on computer vision* , pp. 4015–4026.

Meyer, L., Gilson, A., Schmid, U., and Stamminger, M. (2024) *Fruitnerf: A unified neural radiance field based fruit counting framework*. In: *2024 IEEE/RSJ International Conference on Intelligent Robots and Systems (IROS)* , pp. 1–8. IEEE.

Mildenhall, B., Srinivasan, P.P., Tancik, M., Barron, J.T., Ramamoorthi, R., and Ng, R. (2021) *Nerf: Representing scenes as neural radiance fields for view synthesis*. *Commun. ACM*, **65**, 99–106.

Ronneberger, O., Fischer, P., and Brox, T. (2015) *U-net: Convolutional networks for biomedical image segmentation*. In: *International Conference on Medical image computing and computer-assisted intervention* , pp. 234–241. Springer.

Schonberger, J.L. and Frahm, J.-M. (2016) *Structure-from-motion revisited*. In: *Proceedings of the IEEE conference on computer vision and pattern recognition* , pp. 4104–4113.

Schubert, E., Sander, J., Ester, M., Kriegel, H.P., and Xu, X. (2017) *DBSCAN revisited, revisited: why and how you should (still) use DBSCAN*. *ACM Transactions on Database Systems (TODS)*, **42**, 1–21.

Seitz, S.M., Curless, B., Diebel, J., Scharstein, D., and Szeliski, R. (2006) *A comparison and evaluation of multi-view stereo reconstruction algorithms*. In: *2006 IEEE computer society conference on computer vision and pattern recognition (CVPR'06)* , pp. 519–528. IEEE.

Sun, C., Choe, J., Loop, C., Ma, W.-C., and Wang, Y.-C.F. (2025) *Sparse Voxels Rasterization: Real-time High-fidelity Radiance Field Rendering*. In: *Proceedings of the Computer Vision and Pattern Recognition Conference* , pp. 16187–16196.

Zhao, J., Geipel, J., Kusnierek, K., and Cui, X. (2025) *InvNeRF-Seg: Fine-Tuning a Pre-Trained NeRF for 3D Object Segmentation*. *arXiv preprint arXiv:2504.05751*.

